Eur. Phys. J. D **21**, 299–309 (2002)
DOI: 10.1140/epjd/e2002-00209-9

THE EUROPEAN PHYSICAL JOURNAL D

Line shape analysis of two-colour photoassociation spectra on the example of the Cs_2 ground state

Ch. Lisdat[a], N. Vanhaecke, D. Comparat, and P. Pillet[b]

Laboratoire Aimé Cotton, CNRS, bâtiment 505, Campus d'Orsay, 91405 Orsay Cedex, France

Received 21 May 2002
Published online 15 October 2002 –

Abstract. Two-photon photoassociation spectra in a Λ-type excitation scheme are analysed under the systematically varied experimental conditions of frequency detunings and laser intensities. Line shape fits are presented as well as the investigation of intensity and detuning dependent line shifts. From both we determine the attained spectroscopic precision, that is corrected for a systematic line shift due to the thermal distribution of atoms in the trap. An energy correction for this effect is given. Information about the feasibility of generating translationally cold molecules in a well defined rotational and vibrational level by the photoassociation process is derived from the analysis.

PACS. 33.70.Jg Line and band widths, shapes, and shifts – 32.80.Pj Optical cooling of atoms; trapping – 34.50.Rk Laser-modified scattering and reactions

1 Introduction

With the development of laser cooling and trapping techniques, experiments with ultra cold (<1 mK) and dilute gas samples became possible, leading finally into the quantum degenerate regime and to Bose-Einstein condensation. These condensed or thermal atomic clouds allow studies of atomic collisions [1–4] and precise determination of molecular states with extraordinary properties by photoassociative spectroscopy [5,6].

In the photoassociation process, two colliding ground-state atoms absorb a photon and form an electronically excited molecule. This molecule may decay by spontaneous emission in two atoms, that have usually higher kinetic energy than before and leave rapidly the atomic cloud, or may form a translationally cold molecule in the ground or lowest triplet state [7]. A sample of molecules in a well defined rotational-vibrational level would be interesting for further experiments. Unfortunately, spontaneous emission leads to a distribution of populated levels.

Of course, the photoassociation (PA) schemes are not restricted to the interaction of one light field with the atomic sample, but more sophisticated schemes with multiple photon absorption and emission can be considered. In this way even more molecular states become accessible.

In the case of two-colour PA a photon from each field can be absorbed or the absorption of the first photon can be followed by the stimulated emission of a second photon into the other laser field (termed Λ-like process). The first approach was for example successfully used for the enhancement of the formation of cold molecules [8], while the second Λ-like schemes were used for high resolution spectroscopy in thermal [9–13] atomic clouds and Bose-Einstein condensates [14]. Scattering properties and potential curves were determined with high precision.

Nevertheless, the PA approach suffers from the non-negligible energy distribution of colliding atoms, which leads in general to asymmetric spectral line profiles and line shifts [15,16]. These can only be avoided by PA experiments with quantum degenerate ensembles [14] or by completely different approaches such as spectroscopy on molecular beams [17].

Information about the energy distribution of atoms in the cloud is contained in the line shapes of the observed PA transitions. Thus an investigation of the line profiles can be used to derive collision properties, allowing better knowledge of the spectroscopic precision. Moreover, manipulation of the collisional wave function becomes possible by use of optically induced Feshbach resonances [18].

While photoassociation line shapes were the subject of several investigations in the case of one-photon PA and were even used to determine quantities such as the ground state scattering length [19–22], fewer investigations have been reported for two-photon PA.

By performing two-colour PA in a Λ-scheme within a Cs magneto-optical trap we have measured several rotational series of the lowest electronic states of Cs_2, which correlated to the atomic asymptote $6\,^2S_{1/2} + 6\,^2S_{1/2}$. The experimental approach is described in Section 2. In this article we will compare one of those series with line shape

[a] Current address e-mail: christian.lisdat@ptb.de
[b] e-mail: pierre.pillet@lac.u-psud.fr

simulations based on the formalism developed by Bohn and Julienne [16] (Sect. 3), while the spectroscopic interpretation of the measured levels in terms of potential curves will be the subject of a subsequent publication.

The measurements were done under different experimental conditions. Spectra were recorded with quasi resonant excitation of the intermediate level of the Λ-scheme and for different detunings, as well as for several different intensities of the PA light fields. In Section 4 we discuss the behaviour of the spectra as both parameters are varied. From this analysis, line shifts due to the atomic energy distribution in the MOT are determined for our experimental conditions and the uncertainty of the necessary correction of level energies is determined (Sect. 4.3).

From these results we can deduce the mechanism, which leads to the Cs_2 molecule production and if the formation of a molecular sample in a single well defined level is feasible under the chosen experimental conditions. Therefore, this work follows and investigates more in detail a first series of experiments, which were already accomplished in our group [23]. The results are summarized in Section 5.

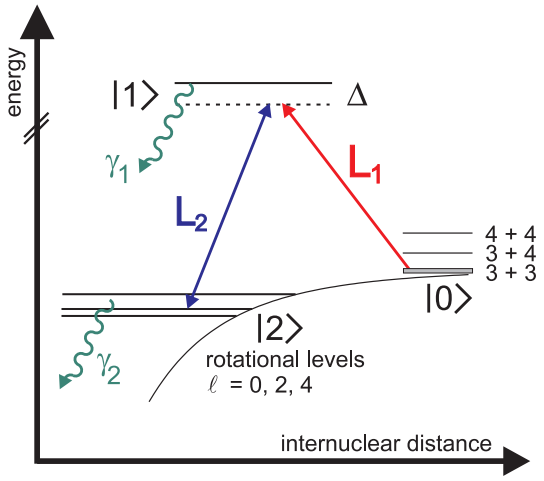

Fig. 1. Coupling scheme for two-photon PA. The two laser fields are denoted L_i, Δ is the detuning of L_1 with respect to the level $|1\rangle$. The vibrational level at the ground state asymptote with its rotational structure is called $|2\rangle$. The grey shaded area above the lowest hyperfine asymptote $3+3$ indicates the thermal distribution of atoms in the MOT ($|0\rangle$). For later use possible loss channels with rates γ_i are shown as well.

2 Experimental approach

2.1 Photoassociation scheme

Since the experimental setup was described in detail before [7,24,25], we will describe here only the main outline and recent changes.

Cesium atoms are cooled and trapped in a standard magneto-optical trap (MOT) loaded from Cs background vapour with a pressure of about 2×10^{-7} Pa. The MOT is operated in dark SPOT configuration [25]. In this way an atomic cloud of 5×10^7 atoms with a temperature of $\sim$200 μK is formed. To perform the photoassociation experiments considered here, the atomic cloud is continuously illuminated by two laser fields L_1 and L_2 with frequencies, ν_1 and ν_2, respectively. The field L_1 is provided by a Ti:Sa laser with maximum output power of 1 W, while L_2 is generated by a DBR laser diode of 100 mW optical power.

The field L_1 couples the collision state of two cold Cs atoms to the $v=1$ vibrational level of the attractive 1_u 6 $^2S_{1/2}$ + 6 $^2P_{3/2}$ electronic state (Fig. 1). A detailed discussion of the spectroscopy of the state 1_u is found in [25]. From reference [25] we know that each vibrational band of the 1_u state is a manifold of levels strongly coupled by rotation and hyperfine structure. As initial collision state the lower hyperfine asymptote $(f_1=3)+(f_2=3)$ was chosen for its strong PA spectra of the $v=1$ level [25].

To avoid complications during the analysis by blended lines, a free standing line in this vibrational band was selected (in [25], Fig. 5 at 0 GHz). It can be deduced from previous investigations of the hyperfine and rotational coupling in the state 1_u that the wave function of this level $|1\rangle$ is mainly characterized by the quantum number $f'=7$ and $m_{f'}=7$. The quantum number f describes the total molecular angular momentum without rotation of the nuclei ℓ, m_f is the projection of f on the molecular axis. For symmetry reasons, only even ℓ values contribute to $|1\rangle$.

The frequency ν_2 of the field L_2 is chosen so that it couples the state $|1\rangle$ to a vibrational level $|2\rangle$ located 18 GHz below the atomic asymptote $(f_1=3)+(f_2=3)$. Its classical outer turning point is around $35a_0$. This level is a mixture of the electronic $X\ ^1\Sigma_g^+$ and $a\ ^3\Sigma_u^+$ states, which is generated by the hyperfine coupling. $|1\rangle$ is coupled to levels with even ℓ only, since ℓ is maintained during the emission or absorption of photons and is fairly decoupled from the electronic motion at large internuclear distance in the ground states [17]. Furthermore, electronic selection rules for $\Delta f=f'-f=0,\pm1$ allow only coupling to levels in the $f=6,7,8$ hyperfine manifold. $f=7$ and 8 are ruled out, because the symmetry of their wave functions is purely *ungerade* for even ℓ, since only one hyperfine potential curve exists for each case and these correlate at short distances to the $a\ ^3\Sigma_u^+$ state. Therefore, coupling to the 1_u excited state by electronic dipole transitions is forbidden. In contrast, g/u symmetry breaking appears in the $f=6$ subspace due to hyperfine coupling [26] of the $X\ ^1\Sigma_g^+$ and $a\ ^3\Sigma_u^+$ states.

At short distances the degeneracy of m_f is removed by the increasing spin-orbit interaction [27,28]. Since the intermediate level $|1\rangle$ is described by $m_{f'}=7$, only levels with $f=6, m_f=6$ are populated in $|2\rangle$.

Due to the selection rules discussed above, from the large number of potentials only three potential curves are coupled to the excited state $|1\rangle$. The observed spectra are in this way significantly simplified and show well separated rotational-vibrational lines.

For fixed frequency ν_1, frequency ν_2 is tuned and the formation rate for Cs_2 molecules in the $X\ ^1\Sigma_g^+$ or

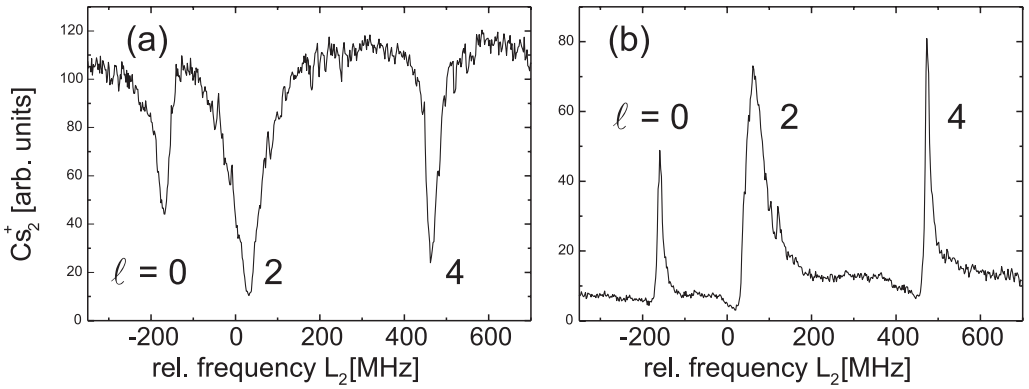

Fig. 2. Rotational series of a vibrational level 0.6 cm^{-1} below the hyperfine asymptote $3 + 3$ measured by two-colour PA. (a) L_1 excites resonantly the intermediate level $|1\rangle$ while L_2 is tuned. Frequencies are measured relative to the atomic asymptote with a fixed offset for all shown spectra in the paper. (b) Same as (a), but L_1 is detuned about 20 MHz to higher frequencies.

$a\ ^3\Sigma_u^+$ state is observed. Molecules are observed by ionisation with a pulsed laser and detection of the Cs_2^+ ions with a pair of micro channel plates [24].

Two processes are likely to form Cs_2 dimers in the X or a state: (i) the excited level $|1\rangle$ of the 1_u can be populated *e.g.* by L_1 in direct PA process. Spontaneous decay of this state will form a distribution of populated levels in the electronic states dissociating to the asymptote $6s+6s$. (ii) $|2\rangle$ is populated by a stimulated Raman transition and molecules in these levels are detected directly, or the population is redistributed before detection by non-resonant reabsorption and following decay to other molecular levels.

Two situations are experimentally easily distinguishable, namely when L_1 excites resonantly the level $|1\rangle$ or when it is detuned by Δ from the resonance:

$$\Delta = E_1 - h\nu_1. \qquad (1)$$

Here, E_1 labels the energy of level $|1\rangle$ with respect to the asymptote $3 + 3$ and h is Planck's constant. In agreement with [16], $\Delta > 0$ corresponds to a *red* detuned laser field.

Examples for spectra under both conditions are shown in Figure 2. Figure 2a is taken with L_1 on resonance, which produces a large Cs_2^+ ion signal by direct PA in absence of any resonant coupling of $|1\rangle$ and levels of $|2\rangle$ by L_2. When the field L_2 resonantly couples the levels $|1\rangle$ and $|2\rangle$, the Cs_2^+ ion signal is strongly reduced due to a two-photon dark resonance. In a previous paper [23] this process was termed as frustrated PA. Three rotational lines are visible in Figure 2a as deep dips in the ion signal.

In Figure 2b, obtained with L_1 detuned from resonance, only a very low signal of direct PA is visible. Now, around the two-photon resonances three narrow and asymmetric lines are visible. On the low frequency side of those lines a slight decrease of the ion signal is visible, leading to a Fano-like line shape with a sequence of maximum and minimum.

The reference of the frequency scale is the same in all figures in this paper.

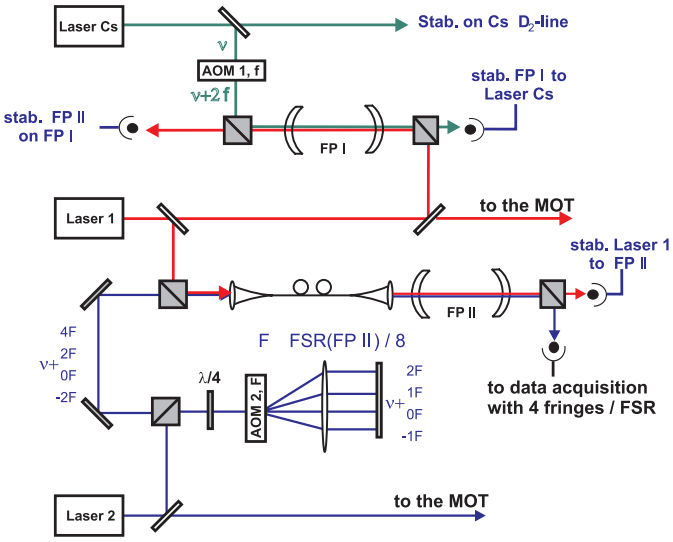

Fig. 3. Setup of the laser system used for the two-colour photoassociation spectroscopy. A detailed description is given in the text.

2.2 Laser spectrometer

To determine the position of the observed ground state levels with respect to the atomic asymptote it is necessary to measure the difference $\Delta\nu = \nu_1 - \nu_2$ with high precision. Small $\Delta\nu$ can easily and most efficiently be determined by rf-techniques, and this technique has been applied in many experiments. For $\Delta\nu$ in the order of several cm^{-1}, however, this becomes unpractical or impossible. For this reason we measure $\Delta\nu$ with a confocal Fabry-Perot interferometer FP II with a previously precisely calibrated free spectral range (FSR) of ∼750 MHz. The whole setup is shown in Figure 3. Light from both L_1 and L_2 is mode-matched by a polarization maintaining single-mode fibre before being fed into FP II to avoid any detuning of the two detected fringe systems due to misalignments. We modulate L_2 with an acousto-optical modulator (AOM 2), which adds side bands to ν_2, that are separated by ∼187.5 MHz ≡ FSR/4.

L_1 is locked on a transmission of FP II, which is tunable by a piezo to adjust the detuning Δ. When ν_2 is tuned to record a spectrum, we know that the corresponding fringes are separated by an integer number of quarters of the free spectral range from ν_1. This number is calculated from the values of ν_1 and ν_2 measured by comparison with an iodine absorption spectrum [29]. $\Delta\nu$ is then determined by linear interpolation between two transmissions of FP II plus the integer number times a quarter of the free spectral range.

For good long term stability of ν_1, FP II is stabilized by means of another coupling cavity FP I tunable by a piezo crystal. FP I's frequency comb is fixed, since it is stabilized itself on a laser locked on a Cs saturated absorption signal. To reach arbitrary values of ν_1, AOM 1 in double pass configuration provides an interpolation between the fringes of FP I.

Analyzing the spectrometer we have found that we can determine $\Delta\nu$ with an accuracy better than 3 MHz for $|\Delta\nu| < 3$ cm^{-1}. The uncertainty is given by the nonlinearity of the scan, errors in the determination of the fringe positions and the uncertainty of the free spectral range of FP II due to its calibration and the dependence on the environment. Both calibration and stability of FP II can be improved in the future.

We will examine in Section 4 if the frequencies of the minima and maxima visible in Figure 2 depend on experimental parameters such as the detuning Δ or the intensity of the light fields. Additionally, the spectra will be compared with simulations based on the formalism introduced in the next section. In this way we are able to determine possible systematic line shifts due to the low but finite temperature of the atoms in the trap as they were observed in single photon PA [19]. The exact definition of what we refer to as line shifts is given at the end of Section 4.1.

3 Theory

In this section, we discuss briefly the formalism developed by Bohn and Julienne [15,16] for the description of photoassociation line shapes. The expression given in [16] for two-colour PA is generalized for the case we treat here with one bound excited state coupled to three energetically non-degenerate molecular levels in a ground state potential. At the end of this section we explore the range of validity of the Wigner threshold law and a suitable parameterization of the energy dependence of the Franck-Condon overlap between the collision and bound wave function.

In [16] expressions for various scattering amplitudes S_{ij} were developed that can be connected to experimentally observables such as the trap loss or the formation of molecules. Taking for example the situation sketched in Figure 1 and assuming that we have only one level in the manifold of $|2\rangle$ one can calculate the Cs_2^+ ion signal by the sum of the squares of the scattering amplitudes S_{01} and S_{02}.

To calculate the Cs_2^+ signal, Franck-Condon factors for the spontaneous decay to bound molecular levels and the ionizing efficiencies must be taken into account. In principle they can be calculated [30], but since they give only proportionality factor for a set of fixed molecular levels, they can be later introduced as a single global amplitude factor. S_{01} is given by [16]:

$$S_{01} = \frac{-\mathrm{i}\hbar\sqrt{\gamma_1 \Gamma}\,(\delta + \mathrm{i}\hbar\gamma_2/2)}{(\Delta' + \mathrm{i}\hbar(\gamma_1+\Gamma)/2)\,(\delta + \mathrm{i}\hbar\gamma_2/2) - \hbar^2\Omega^2} \tag{2}$$

with

$$\delta = E - (e - h\Delta\nu), \quad \Delta' = E - (\Delta + \varepsilon) \tag{3}$$

ε is the light shift of $|1\rangle$ coupled to the continuum by L_1 (E_1 in [16]), e is the energy of the level $|2\rangle$ with respect to the asymptote $(f_1 = 3) + (f_2 = 3)$. The kinetic energy of the colliding atoms is called E.

$$\Gamma = 2\pi\hbar\,|\langle 1|\mathbf{E}_1 \cdot \mathbf{d}|0(E)\rangle|^2 \tag{4}$$

describes the excitation rate by L_1 from an energy-normalized continuum state $|0(E)\rangle$ to the molecular level $|1\rangle$, and

$$\Omega = \langle 1|\mathbf{E}_2 \cdot \mathbf{d}|2\rangle\,/\hbar \tag{5}$$

is the molecular Rabi frequency with the electric fields $\mathbf{E}_1$ and $\mathbf{E}_2$ for the lasers L_1 and L_2 and the dipole moment $\mathbf{d}$. The other quantities were already defined in Section 2.1 and Figure 1.

The expression in equation (2) gives the complete molecule formation rate only in the case of negligible loss rate γ_2, otherwise S_{02} will also contribute to it. In the experiment considered here, γ_2 is due to molecules that drop out of the interaction zone, are reexcited by non-resonant absorption of a photon from L_1 or the trap lasers [31], or transferred to other molecular levels by inelastic collisions. All effects lead generally to very small rates in comparison with $\gamma_1 \approx 18$ MHz, which is determined by the lifetime of $|1\rangle$ [32]. Therefore, we will neglect in the following losses from $|2\rangle$. The validity of neglecting γ_2 will be further justified in Section 4. The interaction of L_2 and thus the reexcitation to $|1\rangle$ is already taken into account in equation (2) and provides no additional loss rate γ_2.

In this case ($\gamma_2 \approx 0$), we see there is always a frequency difference $\Delta\nu$ for given E so that S_{01} in equation (2) becomes zero and thus the molecule formation and Cs_2^+ ion signal drops to zero. In this way, we have already developed a qualitative understanding of the spectra in Figure 2a.

Furthermore, this behaviour does not depend on Ω or Γ. Averaging over E or a considerable loss rate γ_2 will lead to a non-zero signal, but nevertheless the characteristics of a dark resonance between the continuum state and state $|2\rangle$ are evident.

For the observed rotational levels in Figure 2 we find that equation (2) is not sufficient, since we observe three levels with energies e_1, e_2, and e_3 that are close or even blending within the observed line width. We have thus

generalized equation (2) following the method given in [16] to a set of in total four bound levels, of which three represent the rotational levels with $\ell = 0, 2, 4$ and with corresponding detunings δ_1, δ_2, and δ_3.

Following equation (2.20) in [16] one defines the reduced **K**-matrix

$$\mathbf{K}^{\mathrm{red}} = \mathbf{K}^{\mathrm{oo}} - \mathbf{K}^{\mathrm{oc}}(\tan\mathbf{n} + \mathbf{K}^{\mathrm{cc}})^{-1}\mathbf{K}^{\mathrm{co}} \tag{6}$$

with submatrices

$$\mathbf{K}^{\mathrm{oo}} \equiv \mathbf{0}$$

$$\mathbf{K}^{\mathrm{co}} = \mathbf{K}^{\mathrm{oc}\dagger} = \sqrt{\hbar}\begin{pmatrix} \sqrt{\Gamma/2} & \sqrt{\gamma_1/2} & 0 \\ 0 & 0 & \sqrt{\gamma_2/2} \\ 0 & 0 & \sqrt{\gamma_2/2} \\ 0 & 0 & \sqrt{\gamma_2/2} \end{pmatrix} \tag{7}$$

$$\tan\mathbf{n} + \mathbf{K}^{\mathrm{cc}} = \begin{pmatrix} \Delta' & \hbar\Omega_1 & \hbar\Omega_2 & \hbar\Omega_3 \\ \hbar\Omega_1 & \delta_1 & 0 & 0 \\ \hbar\Omega_2 & 0 & \delta_2 & 0 \\ \hbar\Omega_3 & 0 & 0 & \delta_3 \end{pmatrix}.$$

From $\mathbf{K}^{\mathrm{red}}$ one can calculate the scattering matrix $\mathbf{S}^*$

$$\mathbf{S}^* = \mathrm{e}^{\mathrm{i}\eta}\frac{1 + \mathrm{i}\mathbf{K}^{\mathrm{red}}}{1 - \mathrm{i}\mathbf{K}^{\mathrm{red}}}\mathrm{e}^{\mathrm{i}\eta} \tag{8}$$

($\mathrm{e}^{\mathrm{i}\eta}$ is a 4×4 diagonal matrix and contains the elastic phase shifts) and identify the element S^*_{01} when neglecting all terms including γ_2:

$$S^*_{01} = \frac{\mathrm{i}\hbar\sqrt{\gamma_1\Gamma}\,\delta_1\delta_2\delta_3}{(\Delta' + \mathrm{i}\hbar(\gamma_1+\Gamma)/2)\,\delta_1\delta_2\delta_3 - \hbar^2(\Omega_1^2\delta_2\delta_3 + \Omega_2^2\delta_1\delta_3 + \Omega_3^2\delta_1\delta_2)}. \tag{9}$$

The similarity of equations (2, 9) is obvious as the symmetric appearance of quantities Ω_i and δ_i corresponding to the three rotational levels with e_i.

To calculate the line profiles, it is finally necessary to average over the energy distribution of Cs atoms in the MOT, for which we assume a Boltzmann distribution $\exp(-E/k_{\mathrm{B}}T)$ with the temperature T and Boltzmann's constant k_{B}.

Since we are dealing with relatively high temperatures of $\sim$200 μK, several partial waves ℓ can in principle contribute to the signal. For symmetry reasons, only even ℓ couple with the intermediate level $|1\rangle$. We restrict our analysis to partial waves s and d, higher ℓ being omitted due to the growing centrifugal barrier. The relative population of the partial waves is given by the factor $2\ell + 1$. We find the expression for the number of Cs dimers N:

$$N \propto \sum_{\ell=0,2}(2\ell+1)\int_0^\infty \mathrm{d}E\exp(-E/k_{\mathrm{B}}T)\,|S^*_{01}(\ell, E)|^2\,. \tag{10}$$

Averaging over the temperature it must be considered that S^*_{01} depends through the rate Γ_ℓ on the collisional partial wave and the collision energy E (Eq. (4)). The energy dependence of Γ_ℓ is well described by an energy-dependent Franck-Condon density. For low E this variation can be parameterized by the Wigner threshold law $E^{\ell+0.5}$. Unfortunately Wigner's expression will break down for s-wave scattering in the case of Cs at very low energies of a few 10 nK due its large scattering lengths and C_6 dispersion coefficient [19,33].

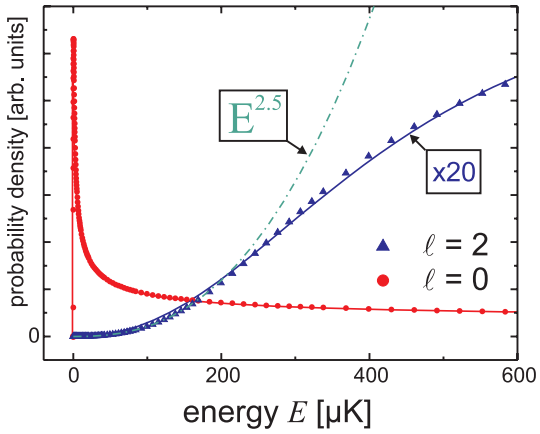

Fig. 4. Points and triangles denote the probability density of the scattering wave function for the asymptote $(f_1 = 3) + (f_2 = 3)$ at $35a_0$ as a function of collision energy E. Solid lines show the parameterization functions used for the line fits. The formulas used are given in Appendix A. The values for $\ell = 2$ are multiplied by 20. Broken line: Wigner like behaviour for d wave collisions.

Thus we have modelled the correct energy dependence of the Franck-Condon density by calculating the probability density of the collision wave function at the Condon point for the excitation of $|1\rangle$ as a function of E (Fig. 4). The wave functions were evaluated with a coupled channel program using potentials, that reproduce within one percent the values for C_6 coefficient and scattering lengths given in [3,34]. We have found by comparison with calculations in a single potential scheme that the variation of the evaluated probabilities as a function of E does not depend strongly on whether a coupled channel calculation is used or not. The same holds for changes of the C_6 coefficient of several percent and the scattering length a, as long as a is of the order of several hundred a_0. Simple analytic functions were adjusted to the calculated values (solid lines in Fig. 4, explicit formulas are given in Appendix A), that were then applied in numerical integration routines in the thermal averaging process.

The probability densities shown in Figure 4 were evaluated at $35a_0$, which corresponds to the Condon point for the excitation of the state 1_u. It can be seen that the dependence on the collision energy E is very distinct for s and d wave collisions. For d waves, the Wigner regime is valid up to much higher temperatures than for $\ell = 0$, which can be seen by comparison with the broken curve.

Since the intensities of the applied light fields are not spatially constant over the atomic cloud, Ω_i and Γ_ℓ are spatially dependent as well. Therefore, we also average over the atom density distribution in the cloud and the profile of the laser beams. The atomic cloud was assumed

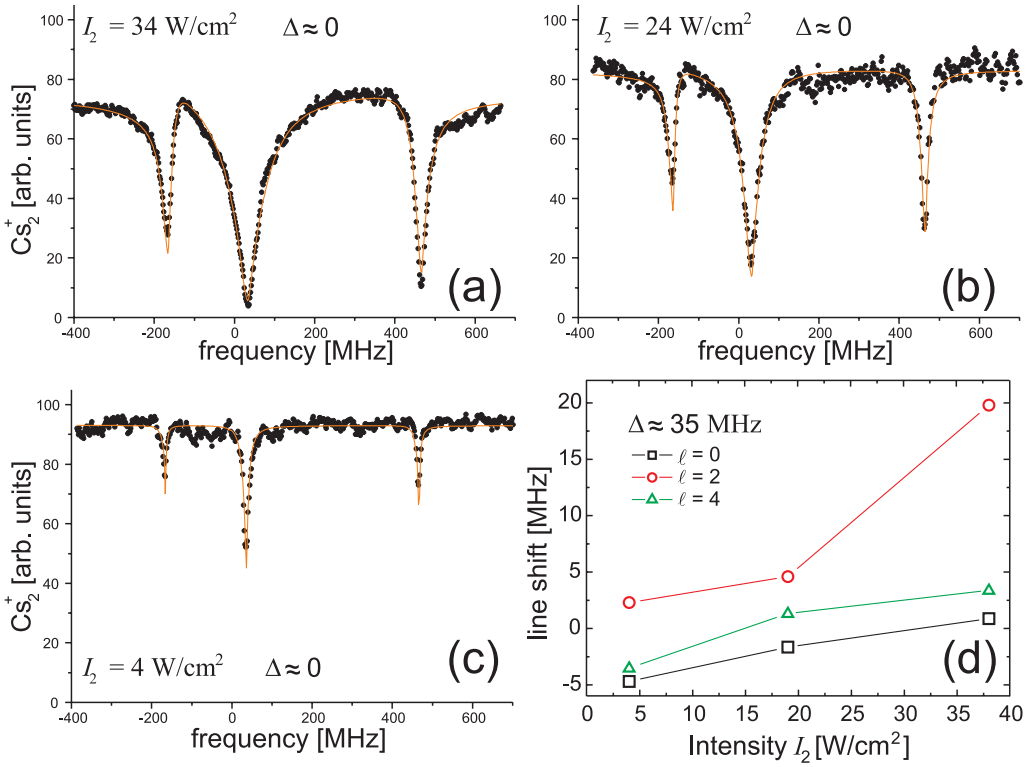

Fig. 5. (a–c) Two-colour PA spectra (dots) measured with different values of I_2 and fixed $I_1 = 74$ W/cm^2 with $\Delta \approx 0$. Solid lines are best line shape fits. (d) Difference between positions of maxima and fitted values for e_i for $\ell = 0, 2, 4$ for L_1 detuned from the intermediate level $|1\rangle$. No intensity dependence was observed for $\Delta \approx 0$, so only results for $\Delta \neq 0$ are shown in (d). Connecting lines are for the sake of clarity and have no physical significance.

to be spherical Gauss-shaped [35], while the laser beams L_1 and L_2 were treated as a cylindrical Gauss profiles with equal and constant waists.

4 Results

In this section we will discuss spectra like in Figure 2 recorded for systematically varied detunings Δ and intensities of L_1 and L_2. They were analyzed in several respects: firstly, the frequencies of maxima or minima were investigated on their dependence on the experimental conditions. No line shape analysis is necessary for this.

Secondly, the measured spectra were compared with simulations. The simulations are based on equations (9, 10) and the averaging processes discussed at the end of Section 3. From those simulations, level energies e_i for the ground state levels were determined that were compared with the values found in the first step. From this we learn about line shifts, which arise from the finite temperature, and about the validity equation (9) to describe the measured spectra. The latter point is important to determine the mechanism which forms the Cs_2 dimers from the variety of possible processes discussed in Section 2.1.

The line shape analysis was performed by means of a non-linear least square fit routine, which varied the parameters in equation (9) to minimize $\chi^2 = \sum_{j=1}^{n}(A_j - S_j)^2/A_j$. n is the number of points in the spectrum, typically about 700, A_j and S_j are measured and simulated amplitude respectively of a give point j with frequencies ν_j. The normalization takes into account the uncertainty of the signal due to statistical noise, which is proportional to $\sqrt{A_j}$. The temperature $T \approx 200$ μK and the parameters for the geometry of laser beams (waists $w \approx 225$ μm) were determined once by a fit in one group of four spectra with different intensities of L_2 and were kept fixed in later fits. The trap size was assumed to be about 300 μm (FWHM). Actually only the ratio of the laser waists w and trap size is relevant for the calculation, which is the reason, why only one of both geometry factors was fitted.

4.1 Intensity dependence

We measured the rotational series shown in Figure 2 with different laser intensities for L_1 and L_2 with L_1 on resonance ($\Delta \approx 0$) and L_1 off resonance, with $\Delta/h \approx 35$ MHz. On resonance spectra were recorded for peak intensities I_1 of 25 W/cm^2 and 74 W/cm^2 (L_1). Under both conditions, intensities of L_2 of $I_2 = 43, 34, 24, 13$ and 4 W/cm^2 were used (Figs. 5a–5c). For $\Delta \neq 0$ three scans were recorded with $I_1 = 43$ W/cm^2 and $I_2 = 38, 19$ and 4 W/cm^2 (line shifts summarised in Fig. 5d).

Since it is not the interest of this work to determine the continuum light shift ε in equation (3), we did not distinguish between ε and Δ but used one fit parameter $(\Delta + \varepsilon)$

which contains both. This is an approximation, which assumes that ε does not strongly depend on the collision energy E. This is indeed true for low E, as it was pointed out in [16]. Furthermore, ε itself is expected to be small here, since ε is proportional to I_1 and the experiments were done with small intensities more than a factor ten lower than the intensity leading to $\varepsilon \approx -15$ MHz in [16]. Furthermore, we know that the Condon point for the excitation of $v = 1$ in the state 1_u is near a maximum of the collision wave function. The irregular wave function, which contributes to the amplitude of ε, will correspondingly have a node at this internuclear distance. For simplicity, we will replace the generalized detuning $(\Delta + \varepsilon)$ with Δ in the following. Common fits of data sets with different intensities I_1 were omitted to avoid influences of the intensity dependence of ε.

Fitting was started with a common fit for the spectra with different I_2 for fixed I_1 in the case of frustrated PA ($\Delta \approx 0$, Figs. 5a–5c). Values for e_i and Δ were adjusted for all spectra in common, as were excitation rates Γ_0 and Γ_2. Ratios Ω_2/Ω_1 and Ω_3/Ω_1 of Rabi frequencies were common parameters, too, while Ω_1 and the proportionality factor in equation (10) were the only individual parameters for each particular spectrum.

The ratios between the values of Ω_i are not completely determined by tensor algebraic expressions for the asymptotic levels considered here. Indeed, the rotational energy changes the wave functions to modify the Franck-Condon factor significantly. Therefore, independent values for Ω_i are necessary, if explicit knowledge about the potential curves is not included in the analysis. Fits including the loss channel γ_2 did not improve the results further. A comparison of fitted parameters is given in Appendix B to demonstrate the consistency of the results.

After having found an already good agreement, each spectrum was fitted alone a second time, using the previously found values for Γ_ℓ and Ω_i allowing an individual variation of e_i and Δ. The second fit led usually to a slight improvement, probably due to not optimal reproducibility of the detuning Δ and frequency scale from scan to scan, leading to differing values of e_i. Nevertheless no changes of parameters appeared, that were greater than 1 MHz for Δ/h and 2 MHz for each e_i/h.

Examples for measurements and fits for the resonant case are shown in Figures 5a–5c. The agreement of experimental results and simulations based on equation (9) is remarkably good. It is clearly visible that the line width decreases strongly with decreasing intensity I_2, while the depth of the dips is not strongly affected. For low intensity (Fig. 5c), the measured dips are not as deep as the simulated ones. This is probably due to averaging over frequency fluctuations of the lasers, especially of L_2, which is provided by a DBR diode with a line width of about 3 MHz. The full width half minimum of these lines is 10 MHz or less. The resonance for $\ell = 2$ shows the largest width and Ω_2 has the largest value, which indicates that the coupling of the level e_2 to $|1\rangle$ is the strongest in the rotational series.

Different tests have shown that the quality of the fits does not strongly depend on the parameterization for the collision wave functions discussed in Section 3 and shown in Figure 4. For these tests, parameterizations for the probability densities calculated for a single scattering channel and different values of a and C_6 from [3,36] were used.

We have not observed any dependence of the line positions on the intensity I_1 or I_2 for L_1 resonant or nearly resonant with $|1\rangle$. This changes dramatically when L_1 is detuned from resonance as in Figure 2b. For fixed Δ, the measured position of the maximum depends strongly on the intensity of L_2. In Figure 5d the difference $h\Delta\nu_{\max,i} - e_i$ between the energy of the maxima in the spectra and the fitted level energies e_i is plotted. We will refer to this difference in the following as line shift. The position of $\ell = 2$ is especially sensitive to the laser intensity. This is explainable since $\ell = 2$ has the strongest coupling to the intermediate level, as we have already deduced from the line widths and the fit parameters Ω_i (see Appendix B). The dependence of the line shift on the laser intensity is a first indication that the process which leads to the Cs_2^+ signal is not mainly based on a stimulated Raman transition, with or without redistribution of the population before detection (Sect. 2.1).

4.2 Detuning

In Section 4.1 we have shown that under our experimental conditions the frustration of the PA signal seems to be preferable to the detuned case for spectroscopic purposes, since the measured line positions do not depend on the applied laser intensities over a wide range. We investigate in this section how the transition from one detuning to another takes place, which means we vary Δ at fixed intensities I_1 and I_2.

The procedure of fitting the spectra was the same as was described in the previous section with the exception that Δ is an individual and Ω_1 a common parameter now. Some results are given in Figures 6a–6c. In Appendix B, some fit parameters are compared with results from Section 4.1. The simulations are again in good agreement with the measurements. The transition from spectra with a high Cs_2^+ ion signal and pronounced dip structures to the inverse situation is clearly visible in part (b). Very asymmetric dispersive line shapes appear, that are nevertheless well matched by the fit. For larger detunings (c), the sequence of minimum – maximum for a rotational line becomes less obvious but remains. It should be remembered that the simulations are based on equation (9) and therefore contain no contribution from population in the levels $|2\rangle$ by the scattering amplitude S_{02}.

Only for large detunings Δ a systematic mismatch of the intensity for lines with $\ell = 4$ is found, which is possibly due to the neglecting of terms S_{02}. Although the amplitude of the signal by losses γ_2 would be indeed negligibly small with a loss rate γ_2 the order of several 10 kHz, a resonant excitation by L_1 to a molecular level may by coincidence lead to a much higher rate γ_2.

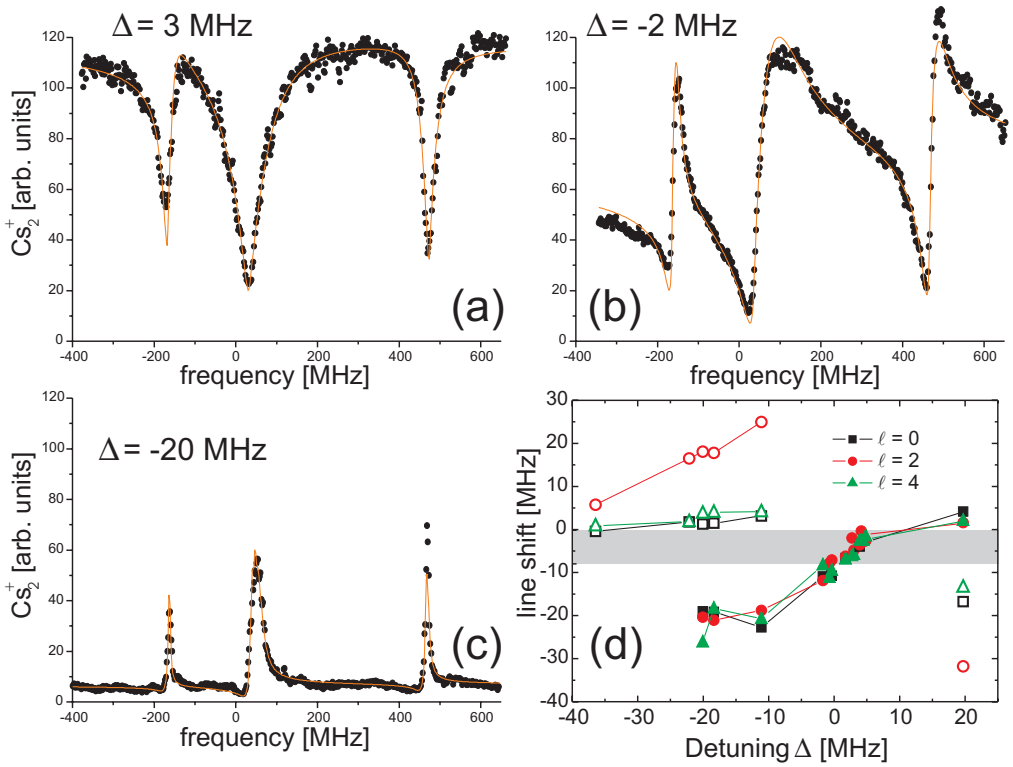

Fig. 6. (a–c) Two-colour PA spectra (dots) measured with different detunings Δ and fixed intensities ($I_1 = 44$ W/cm^2, $I_2 = 28$ W/cm^2). Solid lines are best line shape fits. (d) Shift between positions of maxima and minima and fitted values for e_i for $\ell = 0, 2, 4$ as a function of Δ. Open symbols are related to maxima, full ones to minima. Data from Section 4.1 with $\Delta \approx 0$ is also represented. Connecting lines are again for the sake of clarity and have no physical significance. The grey shaded area is discussed in Section 4.3.

A resonance like this will lead to a local enhancement in a limited energy interval, so that only one rotational line may be enhanced. Nevertheless, the measurements are well described with a formalism including only S_{01}, which means we can indeed in general neglect the amount of population in level $|2\rangle$.

Consequently it does not seem likely that we can, under the conditions discussed here, form a significant number of molecules in a well defined rotational-vibrational level by a stimulated Raman transition. Even if we observe an enhanced loss by reexcitation, this leads to a distribution over many ground state levels by spontaneous decay or even to dissociation of the dimers.

This hypothesis is supported by spectra recorded by detuning the ionisation laser. In a first measurement, single photon photoassociation was used to populate several vibrational levels in the X and a state by spontaneous emission. Consequently, the ionisation spectrum shows a dense structure of lines due to this distribution. In a second measurement, two PA laser fields in the Λ-scheme discussed above were applied, that were tuned and stabilized on a two-photon resonance, while being far detuned from the intermediate level $|1\rangle$. Detuning the ionisation laser, a spectrum very similar to the one measured before was recorded. This indicates again a distribution of population over several molecular levels [30].

Also of interest is the difference between fitted energies and the positions of extrema as a function of Δ and the rotational quantum number ℓ. The determined dependence is shown in part (d) of Figure 6. It can be seen that the minima in the spectra are displaced for all ℓ in the same way within the experimental errors discussed in detail in Section 4.3. At a first glance no such shift would be expected from equation (9), since the dark resonance appears always on the two-photon resonance $\delta_i = 0$. But in this argument the thermal averaging process was neglected. By detuning L_1 different collision energies E of the thermal distribution are preferred by the coupling to $|1\rangle$. Starting out from an other collision energy E leads to changed difference frequencies $\Delta\nu$ at the resonances, since E contributes to the two-photon detuning δ in equation (3).

The shifts in Figure 6d are not symmetric to $\Delta = 0$ for the same reason. We compare the energy $h\Delta\nu_{\min}$ of the minima with the binding energy e_i of the levels derived from the fits. There exists a systematic shift, since selecting a collision state with $E > 0$ is more likely than exciting a pair of colliding atoms with $E \approx 0$ due to the threshold behaviour of Γ discussed in Section 3. By this effect, larger values of $|\Delta\nu_{\min}|$ than the actual $|e_i|$ are determined. It should be recalled that both energies are negative ($\nu_2 > \nu_1$), which leads to negative values for the line shifts in Figure 6d.

If L_1 is on the maximum of the one-photon PA line, we expect the line shift to be equal to Δ, which represents the red shift of the photoassociation line in direct PA by the thermal distribution [19]. We find a line shift of 3 MHz for L_1 on the maximum of the direct PA line, the fit parameter Δ/h is in the order of 4 MHz for those measurements. Simulating the direct PA process (L_1 alone) with the parameters determined from the fit and the equations given in [16], we also find a red shift of the maximum of the line of about 3.5 MHz with respect to the energy difference between the level and the ground state asymptote. This value is in good agreement with fitted value of Δ mentioned above. Of course, this analysis will hold only with relative low intensities I_1, so that no strong saturation effects have to be taken into account [19].

As for the intensity dependence discussed in Section 4.1, the spectral line shifts found for $\Delta \neq 0$ and the maxima are less favourable for precision measurements. Their positions depend also on the detuning, but in a different way for the different rotational lines. As in the case of the intensity dependent shift, the lines for $\ell = 2$ are displaced much more strongly than for the other ℓ values. One can also see at the point at $\Delta/h = 25$ MHz, that the dispersive line shape is inverted with respect to negative Δ. Thus the observed lines for larger detunings are probably not due to stimulated Raman population transfer, but to the population of $|1\rangle$ and spontaneous emission to molecular levels other than $|2\rangle$.

In a dressed state picture of $|1\rangle$, $|2\rangle$ and L_2 the mechanism becomes clear. Even for big detunings $\widetilde{\Delta} = E_1 - e_i - h\nu_2$ of L_2 from the resonance $|2\rangle \rightarrow |1\rangle$, an Autler-Townes doublet exists, although the mixing of the molecular levels is weak. The doublet can be observed by tuning ν_1 for fixed ν_2 [23]. This can also be used for an experimental determination of the Rabi frequencies Ω_i. For big $\widetilde{\Delta}$ the splitting of the Autler-Townes components is mainly determined by $\widetilde{\Delta}$ plus a small repulsion of the dressed states. Then, Cs_2 molecules are probably formed by the excitation by L_1 of the small $|1\rangle$-component in the predominantly $|2\rangle$ dressed state. The intensity dependence in Figure 6d is readily explained by Rabi frequency (Ω_i) dependent repulsion of the dressed levels, which leads to an intensity dependent resonance condition.

The effects discussed here lead to difficulties in spectroscopic analysis under our experimental conditions even in the case of $\Delta \approx 0$, since not all parameters are precisely known and controllable. The achievable precision in the case of frustrated PA will be discussed in the next section.

4.3 Spectroscopic precision

In Section 2.2 we have discussed that the resolution of our laser spectrometer allows us to measure the position of spectral features with an error of a few MHz. In spectra like Figure 5, we can determine the minima in the case of saturation broadened lines to better than ±8 MHz, and at lower intensities, better resolution is possible. In the case of worse signal to noise this uncertainty may be considerably larger. Under these conditions line shifts in the order of 10 MHz and more due to the thermal energy distribution or asymmetric line shapes increase considerably the possible error limits.

Thus we find that under our experimental conditions for spectroscopic analysis an approach with detuned field L_1 must be avoided for the reasons discussed above. More promising is the scheme of frustrated photoassociation, which does not show any significant dependence on the laser intensities used here. The influence of the detuning is much easier to control, since L_1 can be locked on the frequency corresponding to the maximum excitation probability of $|1\rangle$. This condition is relatively well defined when a narrow line for this step is chosen. It was mentioned in the previous section that this is only true for sufficiently low intensities I_1, so that strong saturation is avoided.

By simulations of the one-photon PA process, we can determine the energy range for Δ, in which we allow a ±10% deviation from the maximal signal of direct PA by L_1. This is a reasonable range that we can reproducibly maintain under our experimental conditions. Using Figure 6d this uncertainty in the experimental value of Δ can be transformed in an error limit for the line shift between the measured line positions and the fitted e_i. This margin is indicated in the graph as grey shaded area. In this region we found an uncertainty below ±4 MHz, which is slightly larger than the shift of −3.5 MHz to be corrected.

Besides the uncertainty in the determination of the minimum of the line and the 4 MHz uncertainty discussed above, we have to take into account the error from the laser spectrometer of ±3 MHz. Consequently, we end up with a statistical error of ±10 MHz, if we correct the measured energies by the shift of −3.5 MHz, otherwise the shift adds on the error.

5 Conclusions

In this paper we have analyzed two-colour photoassociation spectra of Cs atoms in a magneto-optical trap. Simulated spectra were fitted to the measurements and the influence of experimental conditions such as laser intensities or the detuning to the intermediate level were investigated.

For the fits we used an expression derived from the formalism developed by Bohn and Julienne [16]. We have shown that simulations and measurements are in very good agreement for a large range of experimental conditions even in the case of nearly blending rotational lines. Fits were done for systematically varied intensities of both optical fields and the detuning Δ. The parameters found by the fitting procedure are consistent.

In this paper, we have discussed more precisely the process already described in a preliminary paper [23]. The transition from frustrated photoassociation *via* the intermediate level $|1\rangle$ to a far detuned regime was investigated, in which sharp peaks appear instead of dips. Those line profiles are well explained by the scattering matrix element S_{01}, which describes losses from $|1\rangle$. Thus we

conclude here that the observed Cs_2^+ ion signal is not due to selective population of a single well defined molecular level. This conclusion is confirmed by simulations of the molecule formation due to S_{02}, which gives no significant contribution.

Despite this general conclusion, PA Λ-schemes in thermal atomic clouds may be used to preferably populate a chosen molecular level. For this purpose, the loss rate γ_2 has to be enlarged with respect to γ_1 by some experimental manipulations. This could be an additional laser field, exciting the population in $|2\rangle$ to a level with an exceptionally good Franck-Condon factor with the vibrational level to be populated. A distribution over rotational levels by spontaneous emission can more easily be avoided by exciting a level with $J' = 0$, that will decay to $J = 1$ levels only due to selection rules. More generally applicable would be a sophisticated transport mechanism, which avoids further coupling of molecules in $|2\rangle$ to the laser fields by spatial displacement.

We found for the frustrated photoassociation that the line positions depend within our experimental resolution only on the detuning Δ of the first field L_1 to the excited level $|1\rangle$, while for the off-resonant situation also an additional dependence on the intensity of the laser fields was found. Consequently, frustrated photoassociation is preferable for spectroscopic purposes under our experimental conditions. We could show that the uncertainty due to the detuning from the resonance of the direct PA is in our experiment below 4 MHz. The systematic shift due to the thermal distribution of atoms in the trap is about -3.5 MHz.

Based on these investigations we will analyse in a further publication the spectroscopic results we have found for a number of rotational vibrational molecular levels below the ground state asymptote of Cs.

An investigation of the modification of ground state wave function by the light-induced embedding of molecular levels in the continuum would be of interest as well. Experiments in this manner were done before with one bound level coupled to the continuum state [18]. The experiment discussed here can be regarded in a comparable manner, since two dressed states are prepared by the molecular levels $|1\rangle$ and $|2\rangle$ and the light field L_2. These levels are then coupled to the continuum by L_1 as an optically induced Feshbach resonance. This is even a double Feshbach resonance due to the doublet nature of the molecular dressed states. The energy splitting between both quasi-bound levels as well as their amplitudes in the dressed states can be varied by the intensity and detuning of L_2. This kind of coupling scheme promises a very rich field for experiments.

The authors thank A. Crubellier and O. Dulieu for many helpful discussions on the Wigner threshold regime and calculations of collision wave functions. Critical reading of the manuscript by D. Tate is also gratefully acknowledged. This work was supported by "Action Concertée Incitative Photonique" of the French research Ministry. This work was also supported by a fellowship for Ch.L. within the "Postdoc-Programme" of the German Academic Exchange Service (DAAD).

Table 1. Selected fit parameters determined in fitting sessions for the intensity dependence of L_2 with intensities for L_1 of $I_1 = 74$ and 25 W/cm^2 and for the session with variable detuning Δ.

Session	$I_1 = 74$ W/cm^2	$I_1 = 25$ W/cm^2	$\Delta \neq 0$
Ω_2/Ω_1	2.0	2.1	2.0
Ω_3/Ω_1	1.2	1.2	1.1
Γ_0	47.2×10^6 s^{-1}	34.7×10^6 s^{-1}	
Γ_2/Γ_0	0.62	0.62	0.10

Table 2. Fit parameters Ω_1, that were determined for the I_2-intensity dependent fits with $I_1 = 74$ and 25 W/cm^2. Values for I_2 are given in W/cm^2, for Ω_1 in 10^6 s^{-1}.

I_2	Ω_1 ($I_1 = 74$ W/cm^2)	Ω_1 ($I_1 = 25$ W/cm^2)
43	94.4	90.4
34	64.7	82.0
24	43.4	78.8
13	27.2	49.4
4	25.8	24.7

Appendix A

The parametrization functions f_ℓ plotted in Figure 4 are calculated by the following expressions:
$\ell = 0$, below 0.8 μK:

$$f_0(E)|_{E<0.8\mu\mathrm{K}} = -69.98456\exp(-E^{0.65575}/0.15241) + 72.22824 - 18.86039E$$

$\ell = 0$, above 0.8 μK:

$$f_0(E)|_{E>0.8\mu\mathrm{K}} = 2.80085 + 71.20469(E + 0.84336)^{-0.53218}$$

$\ell = 2$:

$$f_2(E) = 4.04428(1 - (1 + 9.7731 \times 10^{-7}E^{2.28174})^{-1}).$$

Appendix B

In the following tables parameters determined in different fitting sessions are compared. The shown parameters are taken from common fits of several spectra.

The fitting parameters listed in Table 1 were determined in independent fitting sessions and show good agreement with exception of the ratio Γ_2/Γ_0, which is in the case of the variation of Δ too small compared with the first two values. Though, this discrepancy is not very important and explicable, since the d-wave contribution to the signal amplitude is only in the order of ten percent even for the higher value of the ratio Γ_2/Γ_0.

The fitted values of Ω_1 in Table 2 vary as expected approximately proportional to the square root of the measured laser intensity I_2. The deviations are probably due to errors in the laser power measurements.

References

1. J. Weiner, V.S. Bagnato, S.C. Zilio, P.S. Julienne, Rev. Mod. Phys. **71**, 1 (1999)
2. C. Chin, V. Vuletić, A. Kerman, S. Chu, Phys. Rev. Lett. **85**, 2717 (2000)
3. P.J. Leo, C.J. Williams, P.S. Julienne, Phys. Rev. Lett. **85**, 2721 (2000)
4. A. Kerman, C. Ching, V. Vuletić, S. Chu, C.J. Williams, P.S. Julienne, C. R. Acad. Sci. Paris **4**, 633 (2001)
5. W.C. Stwalley, H. Wang, J. Mol. Spectrosc. **195**, 194 (1999)
6. F. Masnou-Seeuws, P. Pillet, Adv. At. Mol. Opt. Phys. **47**, 53 (2001)
7. D. Comparat, C. Drag, A. Fioretti, O. Dulieu, P. Pillet, J. Mol. Spectrosc. **195**, 229 (1999)
8. A.N. Nikolov, J.R. Enscher, E.E. Eyler, H. Wang, W.C. Stwalley, P.L. Gould, Phys. Rev. Lett. **84**, 246 (2000)
9. E.R.I. Abraham, W.I. McAlexander, C.A. Sackett, R.G. Hulet, Phys. Rev. Lett. **74**, 1315 (1995)
10. C.C. Tsai, R.S. Freeland, J.M. Vogels, H.M.J.M. Boesten, J.R. Gardner, D.J. Heinzen, B.J. Verhaar, Phys. Rev. Lett. **79**, 1245 (1997)
11. H. Wang, A.N. Nikolov, J.R. Ensher, P.L. Gould, W.C. Stwalley, J.P. Burke Jr, J.L. Bohn, Ch.H. Greene, E. Tiesinga, W. Stwalley, P.S. Julienne, Phys. Rev. A **62**, 052704 (2000)
12. K.M. Jones, S. Maleki, L.P. Ratliff, P.D. Lett, J. Phys. B: At. Mol. Opt. Phys. **30**, 289 (1997)
13. J.M. Vogels, R.S. Freeland, C.C. Tsai, B.J. Verhaar, D.J. Heinzen, Phys. Rev. A **61**, 043407 (2000)
14. R. Wynar, R.S. Freeland, D.J. Han, C. Ryu, D.J. Heinzen, Science **287**, 1016 (2000)
15. J.L. Bohn, P.S. Julienne, Phys. Rev. A **54**, R4637 (1996)
16. J.L. Bohn, P.S. Julienne, Phys. Rev. A **60**, 414 (1999)
17. C. Samuelis, E. Tiesinga, T. Laue, M. Elbs, H. Knöckel, E. Tiemann, Phys. Rev. A **63**, 012710 (2000)
18. F.K. Fatemi, K.M. Jones, P.D. Lett, Phys. Rev. Lett. **85**, 4462 (2000)
19. K.M. Jones, P.D. Lett, E. Tiesinga, P.S. Julienne, Phys. Rev. A **61**, 012501 (1999)
20. E. Tiesinga, C.J. Williams, P.S. Julienne, K.M. Jones, P.D. Lett, W.D. Phillips, J. Res. Inst. Stand. Technol. **101**, 505 (1996)
21. R. Napolitano, J. Weiner, C.J. Williams, P.S. Julienne, Phys. Rev. Lett. **73**, 1352 (1994)
22. C.J. Williams, E. Tiesinga, P.S. Julienne, H. Wang, W.C. Stwalley, P.L. Gould, Phys. Rev. A **60**, 4427 (1999)
23. B. Laburthe Tolra, C. Drag, P. Pillet, Phys. Rev. A **64**, 61401(R) (2001)
24. A. Fioretti, D. Comparat, C. Drag, C. Amiot, O. Dulieu, F. Masnou-Seeuws, P. Pillet, Eur. Phys. J. D **5**, 389 (1999)
25. D. Comparat, C. Drag, B. Laburthe Tolra, A. Fioretti, P. Pillet, A. Crubellier, O. Dulieu, F. Masnou-Seeuws, Eur. Phys. J. D **11**, 59 (2000)
26. H. Weckenmeier, U. Diemer, W. Demtröder, M. Broyer, Chem. Phys. Lett. **124**, 470 (1986)
27. F.H. Mies, C.J. Williams, P.S. Julienne, M. Krauss, J. Res. Inst. Stand. Technol. **101**, 521 (1996)
28. S. Kotochigova, E. Tiesinga, P.S. Julienne, Phys. Rev. A **63**, 012517 (2000)
29. *Atlas du spectre d'absorption de la molecule d'iode [11000-14000 cm^{-1}]*, edited by S. Gerstenkorn, J. Vergès, J. Chevillard, Laboratoire Aimé Cotton, CNRS II, Orsay, France, 1982
30. C. Dion, O. Dulieu, D. Comparat, W. Souza de Melo, N. Vanhaecke, P. Pillet, R. Beuc, S. Milošević, G. Pichler, Eur. Phys. J. D **18**, 365 (2002)
31. N. Vanhaecke, W. Souza de Melo, B. Laburthe Tolra, D. Comparat, P. Pillet, Phys. Rev. Lett. **89**, 063001 (2002)
32. P.S. Julienne, J. Vigué, Phys. Rev. A **44**, 4464 (1991)
33. P.J. Leo, P.S. Julienne, F.H. Mies, C.J. Williams, Phys. Rev. Lett. **86**, 3743 (2001)
34. C. Amiot, O. Dulieu, J. Chem. Phys. **117**, 5155 (2002)
35. C. Drag, B. Laburthe Tolra, O. Dulieu, D. Comparat, M. Vatasescu, S. Boussen, S. Guibal, A. Crubellier, P. Pillet, IEEE J. Quant. Electron. **36**, 1378 (2000)
36. C. Drag, B. Laburthe Tolra, B. T'Jampens, D. Comparat, M. Allegrini, A. Crubellier, P. Pillet, Phys. Rev. Lett. **85**, 1408 (2000)